Modifications of heavy-flavor spectra in sqrt[s_{NN}]=62.4 GeV Au-Au collisions

Min He, Rainer J. Fries, and Ralf Rapp

Phys. Rev. C **91**, 024904 — Published 12 February 2015

DOI: 10.1103/PhysRevC.91.024904

Modifications of Heavy-Flavor Spectra in $\sqrt{s_{\rm NN}} = 62.4$ GeV Au+Au Collisions

Min He,[1] Rainer J. Fries,[2] and Ralf Rapp[2]

[1] *Department of Applied Physics, Nanjing University of Science and Technology, Nanjing 210094, China*
[2] *Cyclotron Institute and Department of Physics and Astronomy, Texas A&M University, College Station, TX 77843, USA*

(Dated: January 8, 2015)

We calculate open heavy-flavor (HF) production in Au+Au collisions at $\sqrt{s_{\rm NN}}$=62.4 GeV utilizing a nonperturbative transport approach as previously applied in nuclear collisions at top RHIC and LHC energies. The effects of hot QCD matter are treated in a strong-coupling framework, by implementing heavy-quark diffusion, hadronization and heavy-flavor meson diffusion within a hydrodynamic background evolution. Since in our approach the heavy-flavor coupling to the medium is strongest in the pseudo-critical region (including the effects of resonance recombination), it is of interest to test its consequences at lower collision energies where the sensitivity to this region should be enhanced relative to the initially hotter fireball temperatures reached at top RHIC and LHC energies. We find that the suppression and flow pattern of the non-photonic electrons from heavy-flavor decays at 62.4 GeV emerges from an intricate interplay of thermalization and initial-state effects, in particular a Cronin enhancement which is known to become more pronounced toward lower collision energies.

PACS numbers: 25.75.Dw, 12.38.Mh, 25.75.Nq
Keywords: Heavy Flavor, Quark Gluon Plasma, Ultrarelativistic Heavy-Ion Collisions

I. INTRODUCTION

Heavy quarks (charm and bottom), produced in primordial hard processes in ultrarelativistic heavy-ion collisions (URHICs), experience the entire evolution of the hot fireball formed in these reactions. At high transverse momenta, $p_T \gg m_Q$ (where m_Q is the heavy-quark (HQ) mass), the quenching and subsequent fragmentation of heavy-flavor (HF) jets allows one to study the mass and color-charge dependence of parton energy loss [1]. At low and intermediate p_T, however, gluon radiation is suppressed [2], and heavy quarks become unique "Brownian markers" of elastic thermalization and diffusion processes in the QCD medium, see Ref. [3] for a review. The observation of a remarkable suppression and elliptic flow of HF electrons at top RHIC energy [4–6] and of HF mesons at the LHC [7–12] imply a substantial HF coupling to the medium, being dragged by its collective flow. Different transport models based on perturbative or nonperturbative interactions have been developed to understand these phenomena at RHIC [13–23] and LHC [24–30].

A key question in these investigations is whether the HF coupling to the medium is primarily driven by an increasing temperature (or energy density), or by an increase in coupling strength in the pseudo-critical region of the chiral/deconfinement transition. It is therefore of interest to study how the HF collectivity develops as the collision energy is lowered from top RHIC energy, to reduce the initial temperatures while still encompassing the transition region. In the HF sector, this has recently been realized in the 62.4 GeV run at RHIC [31, 32]. However, it is known from light-hadron spectra that initial-state modifications become increasingly pronounced at lower energies through the Cronin effect, *i.e.*, a nuclear broadening of the initial spectra due to prescattering prior to the hard process. This is important in the quantitative interpretation of, *e.g.*, π^0 suppression at 62.4 GeV, where the nuclear modification factor, R_{AA}, is significantly less suppressed than at 200 GeV [33]. For HF observables a significant Cronin enhancement has been observed in single-electron decay spectra in 200 GeV d+Au collisions [34], which is expected to become larger at lower energies.

The aim of the present paper is to quantify the thermalization effect on HF production in the hot medium at low and intermediate p_T in Au+Au collisions at $\sqrt{s_{\rm NN}}$=62.4 GeV. To this end, we employ our previously developed nonperturbative transport model [22], with medium evolution and initial conditions adapted to this energy and incorporating the Cronin effect in a systematic manner. Specifically, we calculate the $R_{\rm AA}$ and elliptic flow (v_2) of HF electrons and compare the results to recent PHENIX and STAR data. Since our nonperturbative HF diffusion approach is characterized by a maximal interaction strength in the pseudo-critical region [35, 36], its application at lower energies can help to test the validity of this behavior.

Our paper is organized as follows. In Sec. II, we briefly review the ingredients to our model, *i.e.*, the microscopically calculated HF transport coefficients and fits of the macroscopic hydro evolution to bulk-hadron observables at 62.4 GeV (Sec. II A), and discuss in some detail our implementation of the Cronin effect (Sec. II B). In Sec. III, we analyze the interplay of Cronin effect and HF thermalization, including the partitioning of charm and bottom contributions to HF electrons (Sec. III A), and discuss our final numerical results for their $R_{\rm AA}$ and v_2 in the context of recent PHENIX and STAR data (Sec. III B). We summarize and conclude in Sec. IV.

II. HEAVY-FLAVOR TRANSPORT AND INITIAL CONDITIONS

A. Transport Coefficients and Bulk Medium

Our nonperturbative transport model for open heavy flavor in URHICs was introduced in Ref. [22]. A strong-coupling approach is realized in terms of both micro- and macro-physics, with nonperturbative scattering amplitudes for HF interactions in the QGP and hadronic matter, and a hydrodynamic medium evolution, respectively.

In the QGP, HQ interactions with surrounding quarks, anti-quarks and gluons are evaluated using in-medium T-matrices [35, 37], which are obtained in different partial-wave ($l = S, P$) and color channels (e.g., $a = 1, 8$ for $Q\bar{q}$) from a Lippmann-Schwinger equation

$$T_{l,a} = V_{l,a} + \frac{2}{\pi}\int_0^\infty k^2 dk V_{l,a} G_2 T_{l,a} \ , \qquad (1)$$

where G_2 is the uncorrelated two-particle propagator. The integral equation is solved numerically in each channel through discretization and matrix inversion. The potentials, V, are taken as the internal energy computed in thermal lattice-QCD (lQCD), including relativistic corrections. The internal energy tends to give a better agreement with lQCD data than the free energy, for both charmonium correlators [38], and, more importantly for the present purpose, for the HQ diffusion coefficient (see, e.g., Ref. [23]; the latter turns out to be a factor of 2-4 weaker when using the free energy as the potential [35]). The HQ interaction strength in the QGP increases as $T_{\rm pc} \simeq 170\,$MeV is approached from above, inducing resonance correlations.

The resonant $Q\bar{q}$ and Qq T-matrices at $T_{\rm pc}$ are subsequently utilized as a hadronization mechanism in the resonance recombination model (RRM) [39] on a hydrodynamic hypersurface; left-over charm and bottom quarks are hadronized via FONLL fragmentation [40, 41], consistent with the initial spectra in pp. The diffusion of D and B mesons is seamlessly continued in the hadronic phase using effective scattering amplitudes off bulk hadrons (π, K, η, ρ, ω, K^*, N, $\bar{N}$, Δ and $\bar{\Delta}$) [36].

The hydrodynamic evolution is based on the 2+1D ideal hydro code AZHYDRO [42], augmented with a modern lQCD equation of state for the QGP which is matched in a near-smooth transition to a hadron resonance gas (HRG) at $T_{\rm pc}$=170 MeV. The HRG is chemically frozen out at $T_{\rm ch}$=160 MeV. The introduction of a non-vanishing initial radial flow, together with a compact initial entropy density profile, leads to a saturation of the bulk-v_2 close to $T_{\rm pc}$ and mitigates the problems of ideal hydrodynamics in describing the observed bulk-hadron v_2 down to kinetic freezeout at $T_{\rm kin}\simeq$110 MeV. It also appears to aid in the understanding of direct-photon spectra and elliptic flow [43].

In the following, we deploy our approach to study HF transport in Au+Au collisions at $\sqrt{s_{\rm NN}}$=62.4 GeV.

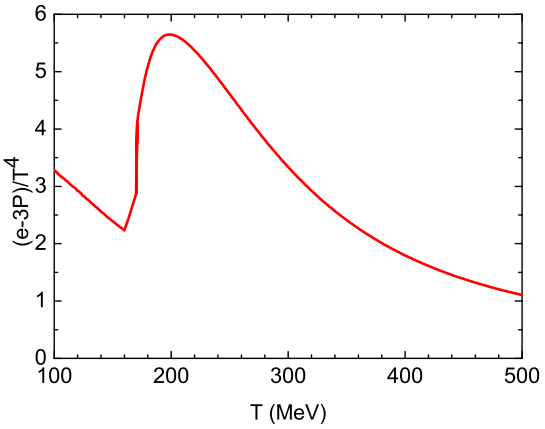

FIG. 1: (Color online) The interaction measure of the EoS used in the present hydro tune as a function of temperature.

The microscopic HF transport coefficients in QGP and hadronic matter are assumed to be the same as at top RHIC and LHC energies, since the quark chemical potential is still rather small at 62.4 GeV, $\mu_q = \mu_B/3 \simeq$ 20 MeV, and the coefficients are rather insensitive to moderate variations in the quark/anti-quark composition (the contributions of Qq and $Q\bar{q}$ scattering are nearly identical, since the weaker interaction strength in the resonant color-triplet relative to the color-singlet channel is essentially compensated by the degeneracy in the former [16, 35]). The particle-antipartilce asymmetry is further washed out in HF electron observables (which we compare to experiment), as these typically involve an average over e^+ and e^- (to improve statistics).

The hydrodynamic bulk evolution is adapted as follows. For the equation of state (EoS), we stay with our fit [44] to the μ_q=0 lQCD results for the QGP part (corrections come in at order $(\mu_q/\pi T)^2$ which are at the sub-percent level). We also assume $T_{\rm pc}$=170 MeV and $T_{\rm ch}$=160 MeV to be unchanged (the latter is within errors of standard HRG fits to observed particle ratios). However, we amend the HRG part of the EoS to accurately reflect the change in hadro-chemistry at the lower energy. While this has practically no impact on the thermodynamic state variables (which again deviate by less than 1% from their 200 GeV counterparts), the $\bar{p}/p$ ratio is significantly affected, decreasing from ca. 0.75-0.8 at 200 GeV to ca. 0.45-0.5 at 62.4 GeV which is noticeable in the absolute norm of our fits to the proton spectra. The resulting interaction measure of our EoS is displayed in Fig. 1. It exhibits the typical maximum slightly above $T_{\rm pc}$, but also starts to rise again at temperatures below $T_{\rm ch}$, which is a consequence of chemical freezeout.

For the initial conditions of the hydro evolution, we follow our tune at top RHIC energy [44] in that we assume the initial entropy density in the transverse plane to be proportional to the binary collision density calculated from the optical Glauber model, $s(x, y; \tau_0) =$

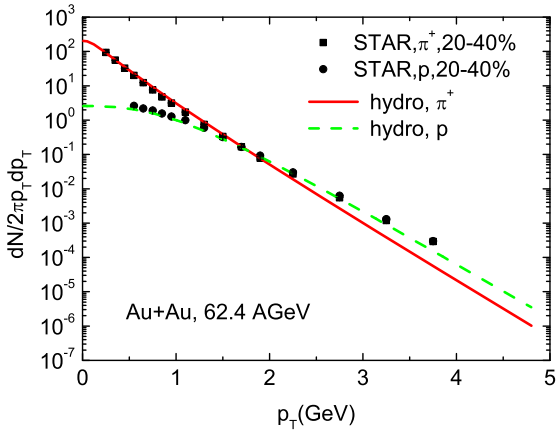

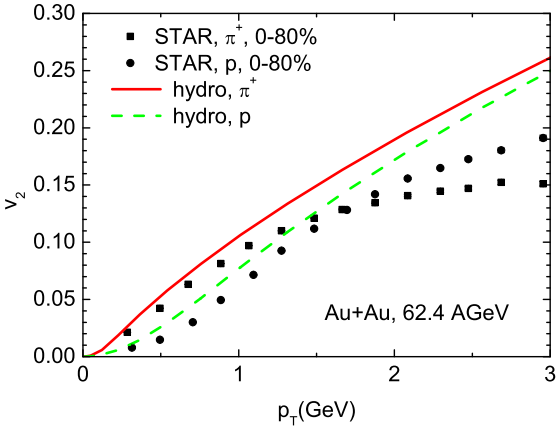

FIG. 2: (Color online) Hydrodynamic fits of π^+ and proton spectra and v_2 to RHIC data [45, 46] using our AZHYDRO tune.

$C(b)n_{\rm BC}(x,y;b)$, where $C(b)$ is an impact-parameter dependent coefficient to ensure the correct charged-particle multiplicity at the respective centrality. Since the initial parton densities are smaller than at 200 GeV, we assume a slightly smaller initial radial flow, $v_T(r;\tau_0) = \tanh(\alpha_0 r)$ with $\alpha_0 = 0.035$ fm^{-1}, and a later thermalization time, $\tau_0 = 0.9$ fm/c. When running our hydro with this initialization, we find that a kinetic freezeout temperature of $T_{\rm kin} = 130$ MeV yields a fair fit to pion and proton spectra out to $p_T \simeq$ 2-3 GeV, cf. Fig. 2. The resulting v_2 tends to slightly overestimate the data already at lower momenta, possibly due to the lack of viscosity in our hydro. However, we recall that the bulk-v_2 is mostly determined by the low-momentum hadrons which constitute the major portion of the total yield; in this regime our fit is not far off and thus should give a reasonable background medium for HF diffusion, within an estimated 20% of accuracy. Since our HF transport coefficients fall off markedly with 3-momentum, most of their interactions with bulk particles occur in the low-p_T regime, where the bulk-v_2 fit is rather close to the data.

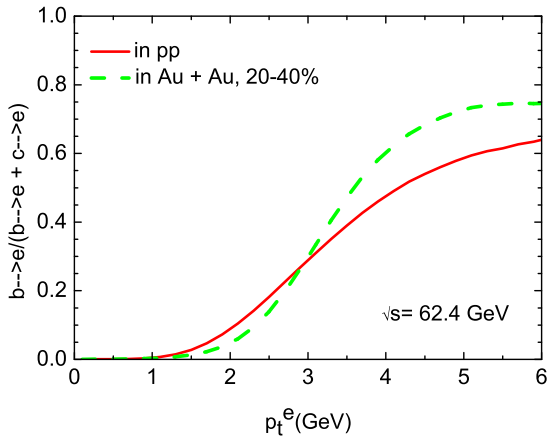

FIG. 3: (Color online) Ratio of electrons from bottom decays to the sum of charm + bottom in pp (red solid line) and 20-40% central Au+Au collisions (including medium effects, green dashed line). Only a slight change in the shape of the p_t^e-dependent ratio is found for Au+Au.

B. Initial HQ Spectra and Cronin Effect

The spectra of D and B mesons in pp collisions at $\sqrt{s_{\rm NN}} = 62.4$ GeV have not been measured yet. For the initial conditions of the HQ spectra, we first generate them from the FONLL software [47] followed by conversion into D- and B-meson spectra using FONLL fragmentation functions [30]. This also defines the denominator of the pertinent nuclear modification factors, R_{AA}. The resulting bottom-to-charm (b/c) cross section ratio of 1.9×10^{-3} is significantly (much) smaller than at top RHIC (LHC) energy, $5 \times 10^{-3}(5 \times 10^{-2})$ [22, 30]. However, when plotting the bottom fraction in the decay electron spectra vs. electron transverse momentum (p_t^e), the result is quite comparable to what we found for top RHIC and LHC energies [22, 30], reaching 0.5 at p_t^e=4-5 GeV, cf. Fig. 3. Thus, the steeper spectra at lower energies decrease the inclusive b/c fraction, while their ratio as a function of p_t^e seems to exhibit rather little dependence on collision energy (a similar trend is found for the B-meson feeddown fraction to J/ψ production). This points at the importance of disentangling bottom and charm contributions also at the lower energies.

Next, we turn to the cold-nuclear-matter (CNM) effects on the HQ spectra, occuring prior to thermalization of the medium. These are usually associated with nuclear shadowing of the parton distribution functions and a Cronin broadening in p_T due to scattering prior to the hard $Q\bar{Q}$ production process. While shadowing of HQ production (especially for charm) presumably plays a significant role in the interpretation of the HF spectra at LHC energy [30], the Cronin effect is believed to become the most important CNM effect toward lower energies [48, 49]; for our $\sqrt{s_{\rm NN}} = 62.4$ GeV calculations we thus focus on the latter. To implement it we follow the

standard procedure of smearing the initial HQ spectra from pp collisions with a Gaussian distribution

$$g(\vec{k}_T) = \frac{1}{\pi\langle k_T^2\rangle}\exp(-\vec{k}_T^2/\langle\Delta k_T^2\rangle_{AA}) \qquad (2)$$

with a variance parameter, $\langle\Delta k_T^2\rangle_{AA}$, characterizing the nuclear broadening. We estimate it following Ref. [21], based on an extension of what has been done before for quarkonia [49, 50]. Assuming the dominance of gluon fusion processes, the nuclear broadening has been parameterized by the ansatz

$$\langle\Delta k_T^2\rangle_{\rm AA}^{Q\bar{Q}} = a_{gN} L_{\rm AB}(x,y;b)\ , \qquad (3)$$

where a_{gN} represents the transverse-momentum squared per path length of a gluon traversing the nuclear medium, and $L_{\rm AB}(x,y;b)$ is the sum of the path lengths of each gluon prior to producing the $Q\bar{Q}$ pair. Typical values extracted from pA/dA spectra at top SPS [51] and RHIC energy [52] are a_{gN}=0.08 GeV^2/fm and a_{gN}=0.1-0.2 GeV^2/fm, respectively [53]. A more systematic energy dependence has been inferred in Ref. [21] through the inelastic NN cross section, $\sigma_{NN}(s)$, as

$$a_{gN}(s) = \Delta^2(\mu)\sigma_{NN}(s)\rho_0\ , \qquad (4)$$

where ρ_0 is the central nuclear density and

$$\Delta^2(\mu) = 0.225\frac{\ln^2(\mu/{\rm GeV})}{1+\ln(\mu/{\rm GeV})}{\rm GeV}^2\ , \qquad (5)$$

characterizes the square-momentum transfer on the gluon per NN collision [54]; assuming its scale dependence given by the HQ mass, $\mu \simeq 2m_Q$, results in approximate agreement with empirical values for a_{gN} at SPS and RHIC. Applying this framework to single HQ spectra yields about half the broadening as for quarkonia, $\langle\Delta k_T^2\rangle_{\rm AA}^{Q} = \langle\Delta k_T^2\rangle_{\rm AA}^{Q\bar{Q}}/2$ [21]. Note that Eq. (3) keeps track of the broadening dependence on transverse position and impact parameter through the effective length $L_{\rm AA}(x,y;b)$ (its explicit form can be found, *e.g.*, in Refs. [21, 50, 53]). This automatically incorporates the binary collision scaling distribution of heavy quarks in the transverse plane. Typical values for $\langle\Delta k_T^2\rangle_{\rm AA}^{Q}$ in central Au+Au collisions at 62.4 GeV come out as $\sim$0.3(1.0) GeV^2 for charm (bottom) quarks. This results in an enhancement of the HF $e^\pm$ spectra in d+Au of up to $\sim$15%. However, already in 200 GeV d+Au an enhancement of up to $\sim$30-40% is observed [34]; for better agreement with phenomenology, we therefore amplify the above estimates of the broadening parameters by a factor of 2 (from here on referred to as default values), *i.e.*, $\langle\Delta k_T^2\rangle_{\rm AA}^{Q} \simeq 0.6\ (2.0)$ GeV^2 for charm (bottom) quarks in central Au+Au collisions. The resulting enhancement in 200 GeV d+Au collisions does not quite reach the observed $\sim$40%, although it is consistent within errors. It is conceivable that final-state effects (*e.g.*, coalescence [55]) provide an additional enhancement in these reactions (which we do not further investigate here). To reflect the uncertainty in our procedure, we vary the broadening parameters within $\pm$50% of the default value.

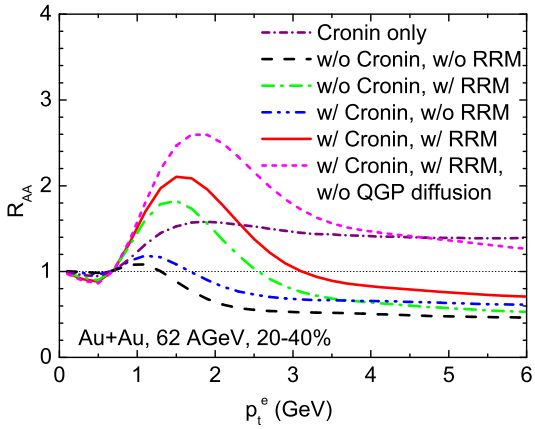

FIG. 4: (Color online) Nuclear modification factor of HF electrons in 20-40% central Au+Au collisions. Different scenarios are compared to illustrate the effects of Cronin broadening (applying the default $\langle\Delta k_T^2\rangle_{\rm AA}^{Q}$ values), resonance recombination (with$\sim$90% integrated coalescence probability for charm and bottom quarks) and QGP diffusion.

III. HF ELECTRON OBSERVABLES

We are now in position to compute HF electron observables in 62.4 GeV Au+Au collisions, using relativistic Langevin simulations through QGP and hadronic matter with the RRM hadronization interface, starting from FONLL HQ initial spectra with Cronin broadening, and semileptonic final-state decays. We will focus on the two standard observables, the nuclear modification factor,

$$R_{\rm AA}(p_T) = \frac{dN_{\rm AA}/dp_T dy}{N_{\rm coll}dN_{\rm pp}/dp_T dy}\ , \qquad (6)$$

and the elliptic flow coefficient,

$$v_2(p_T) = \left\langle\frac{p_x^2-p_y^2}{p_x^2+p_y^2}\right\rangle\ . \qquad (7)$$

A. Cold vs. Hot Nuclear Medium Effects, and Charm vs. Bottom

Let us first study the magnitude and interplay of initial- and final-state effects on the total (charm+bottom) $e^\pm$ $R_{\rm AA}$ in Au+Au collisions, summarized in Fig. 4. When only applying the Cronin broadening at the default value (purple dash-dotted line), the enhancement factor reaches $\sim$1.5 around $p_t^e \simeq 2$ GeV, slowly decreasing thereafter. At $p_t^e \simeq$ 5-6 GeV, the enhancement is essentially due to the then dominant bottom contribution. Next, without any Cronin effect, we compare the result of the HF diffusion with and without applying RRM as a hadronization mechanism. This may serve as a lower estimate of the strong-coupling effects

around the pseudo-critical region. With neither RRM nor Cronin, a weak maximum of the R_{AA} above 1 develops around $p_t^e \simeq 1$ GeV (black dashed line), reflecting the well-known "flow bump" for heavy particles as a consequence of the collectively expanding medium. Upon inclusion of RRM (no Cronin; green dash-dotted line), the net addition of momenta from light quarks from the thermalized medium generates a much more pronounced "flow bump", shifted to a slightly larger $p_t^e \simeq 1.5$ GeV, with a broader structure and a maximum value of $\sim$1.8; the onset of suppression shifts up to above $\Delta p_t^e \simeq 2.5$ GeV. When including the Cronin effect but without RRM (blue dash-dot-dotted line), the maximum structure only moderately enhances over the diffusion-only calculations (much less than due to RRM); however, toward high p_T^e the Cronin effect causes the R_{AA} to level off at a higher value, by about 0.15 (or $\sim$30%). When including both Cronin and RRM (red solid line), the enhancement and broadening of the maximum structure of the electron $R_{\rm AA}$ is further augmented, in a roughly additive manner relative to the "bare" Langevin baseline. Finally, when turning off the HQ diffusion in the QGP (but keeping the Cronin effect and RRM), we confirm that the flow bump mostly develops through resonance recombination. At high p_t^e, on the other hand, RRM induces a suppression relative to the Cronin-only line, characterizing the approach toward equilibrium. This suppression is, however, much weaker relative to the full result (red solid line), reiterating the dominant role of the early QGP phases in the suppression. To summarize this study we find that the dominant effect of RRM (and thus, in a way, of the strong HF coupling to the medium) is the development of a broad flow bump around $p_t^e \simeq 1.5$ GeV, while the Cronin effect mainly manifests itself as an overall increase which is most significant in the suppression regime at higher p_t^e. The elliptic flow (not shown) is essentially unaffected by the Cronin effect, but receives a roughly 30% contribution from RRM, with $\sim$50% from QGP and $\sim$20% from the hadronic phase [23].

To disentangle the effects on the charm and bottom contributions, we show our full results for D and B-meson $R_{\rm AA}$ and v_2 and their individual $e^{\pm}$ decay spectra in Fig. 5. Due to the factor-of-3 mass difference, the D- and B-meson $R_{\rm AA}$ and v_2 are quite different at a given p_T, which is essentially preserved at a given (down-shifted) value of p_t^e. The total $e^{\pm}$ $R_{\rm AA}$ and v_2 largely follow the charm electrons up to $p_t^e \simeq$2-3 GeV (due to charm dominance), while for higher p_t^e the bottom contribution causes a increasing reduction in both suppression and v_2.

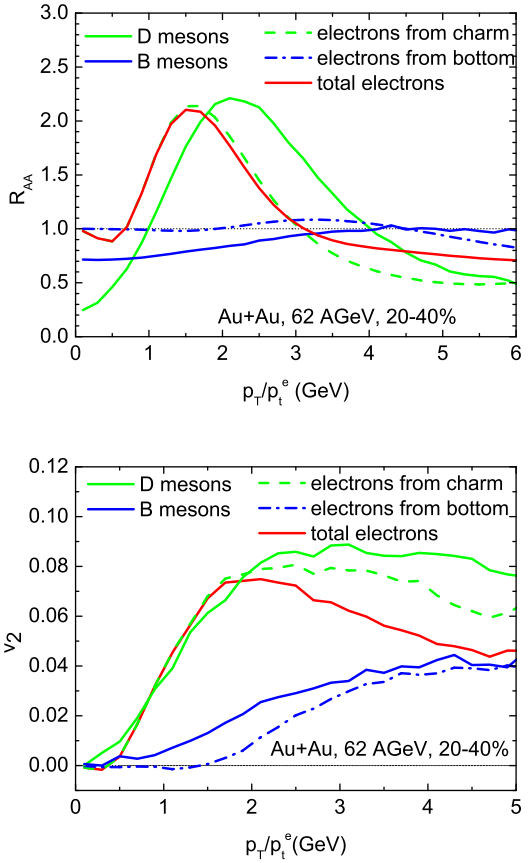

FIG. 5: (Color online) Upper panel: $R_{\rm AA}$ of D mesons, B mesons, their individual and total $e^{\pm}$ decays in 20-40% central Au+Au collisions. Lower panel: the corresponding v_2 results. The default Cronin broadening and $\sim$90% integrated coalescence probability for charm/bottom quarks are applied.

B. Comparison to RHIC Data

We now turn to a systematic comparison of our results to HF electron $R_{\rm AA}$ and v_2 data for different centralities [31]. We assign theoretical uncertainties due to the integrated coalescence probabilities of charm and bottom quarks [30] ($\sim$ 50-90% as in our previous work) and, additively, due to the Cronin effect (default broadening with a $\pm$50% variation), represented by shaded (colored) bands. As discussed in Sec. III A, uncertainties in the coalescence probability prevail in the low p_t^e region, while those from the Cronin effect take over at high $p_t^e \simeq$ 5-6 GeV.

For the HF $R_{\rm AA}$'s, plotted in Fig. 6, our calculations roughly reproduce the data in the two central bins (0-20% and 20-40%), with a tendency to underpredict the yields at higher p_t^e. Given the current experimental errors, it is inconclusive whether the data support a pronounced flow+Cronin bump as present in the calculations. For the more peripheral bin (40-60%) our calculation tends to overestimate the data at low $p_t^e \leq 1$ GeV, where the measured decrease sets in earlier than captured by our implementation of the Cronin effect and/or the collective effects due to the coupling to the hot expanding medium (uncertainties in the pp basline, or pre-equilibrium effects [56], which we do not consider here, may also play a role). Since our previous results for the D-meson $R_{\rm AA}$ at top RHIC energy produce a flow bump which tends to peak at somewhat higher p_T than STAR data in central collisions [57], we believe that an increased collectivity

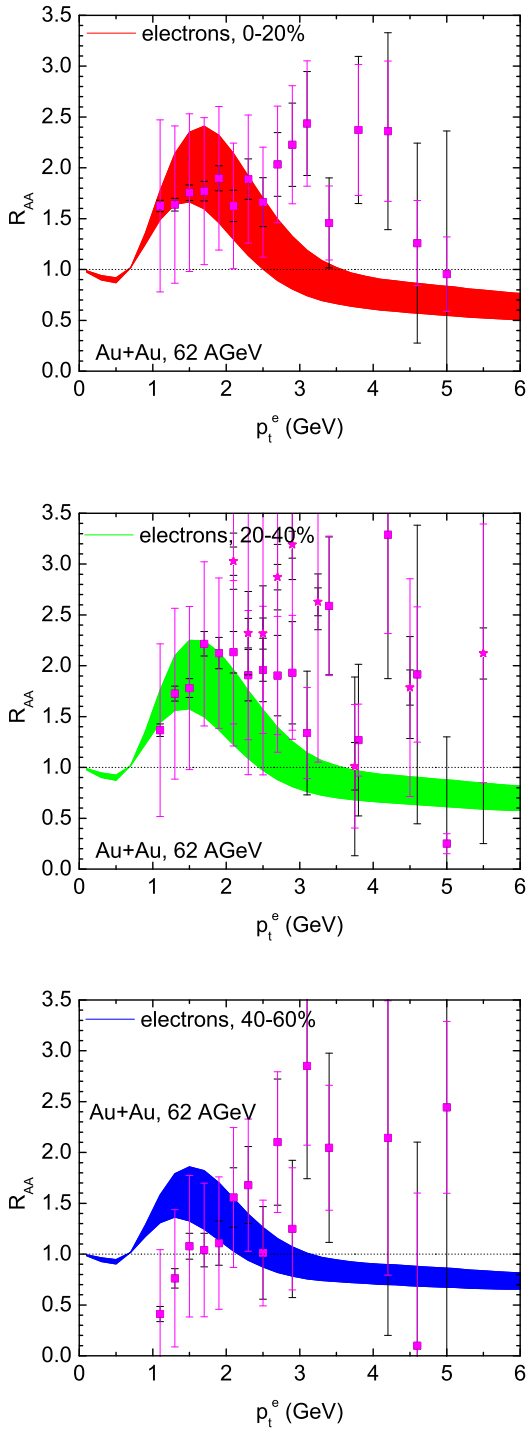

FIG. 6: (Color online) Total HF electron $R_{\rm AA}$ in Au+Au($\sqrt{s_{\rm NN}}$=62.4 GeV) collisions at 0-20% (upper panel), 20-40% (middle panel) and 40-60% (lower panel) centrality. The bands indicate uncertainties due to the total charm- and bottom-quark coalescence probabilities of ∼50-90% and the variation in the Cronin broadening. PHENIX data (filled boxes) are taken from Ref. [31], preliminary STAR data (filled stars in the middle panel) from Ref. [32]. Here and in Figs. 7+8+9 the statistical (systematic) uncertainties of the data are denoted by black (purple) error bars.

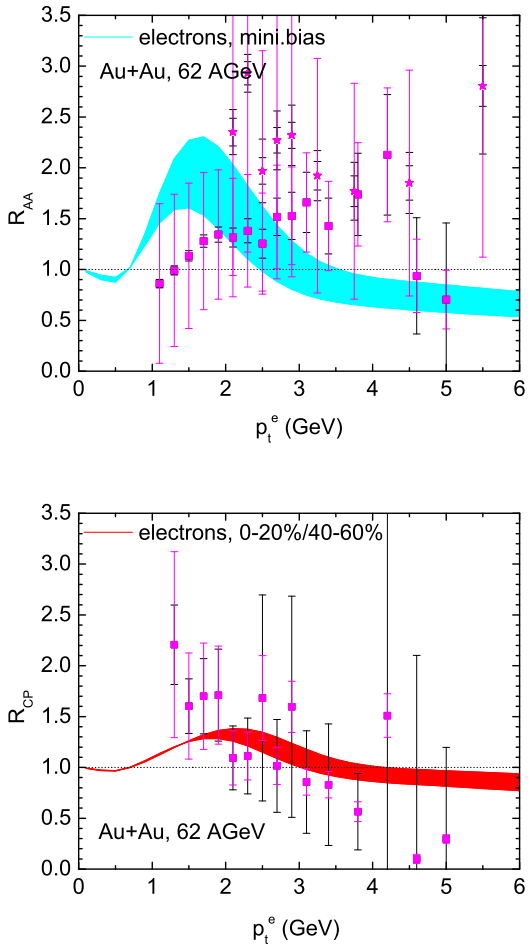

FIG. 7: (Color online) Total HF electron $R_{\rm AA}$ in minimum bias (upper panel) Au+Au($\sqrt{s_{\rm NN}}$=62.4 GeV), calculated from a $N_{\rm coll}$-weighted average of the 0-20%, 20-40%, 40-60% and 60-80% bins, and $R_{\rm CP}$ (lower panel) between 0-20% and 40-60% centrality bins. PHENIX data (filled boxes) are taken from Ref. [31], preliminary STAR data (filled stars in the upper panel) from Ref. [32].

(to deplete the low-p_t^e region) at 62.4 GeV is not a likely mechanism to resolve the discrepancy in the 40-60% centrality bin. For minimum bias (MB) collisions, displayed in the upper panel of Fig. 7, we obtain our result by averaging the above three plus the 60-80% centrality bin, weighted by the binary-collision number, $N_{\rm coll}$, of each bin. The overprediction in the low-p_t^e region found for 40-60% centrality (and probably also for 60-80%) is somewhat mitigated in the MB sample but still present.

We have furthermore computed the central-to-peripheral ratio, $R_{\rm CP}$, obtained from the ratio between the $R_{\rm AA}$'s of 0-20% and 40-60%, and compare it to PHENIX data in the lower panel of Fig. 7. The $R_{\rm CP}$ has the advantage that uncertainties due to the pp baseline spectra largely drop out, but the centrality dependence of the Cronin effect still affects it, although to a lesser extent than in the $R_{\rm AA}$. Our calculated $R_{\rm CP}$ exhibits a

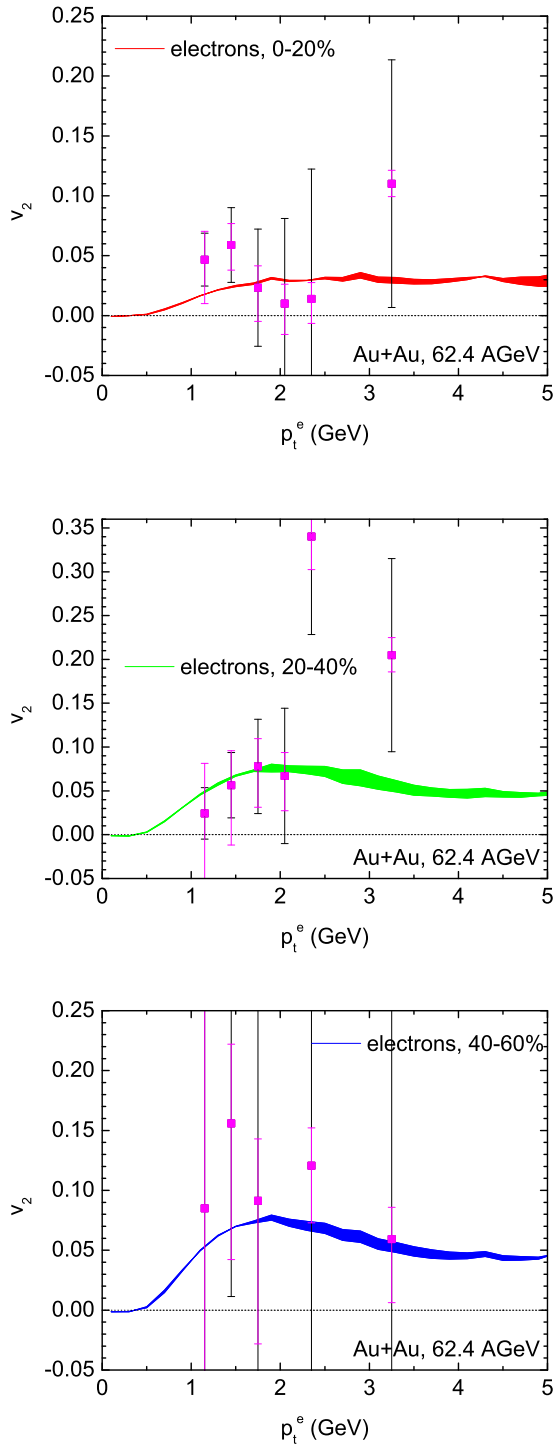

FIG. 8: (Color online) Total HF electron v_2 in 0-20%, 20-40%, 40-60% central Au+Au($\sqrt{s_{\rm NN}}$=62.4 GeV) in the top, middle and lower panel, respectively. The bands denote again the uncertainty in the integrated charm- and bottom-quark coalescence probabilities of ∼50-90%. PHENIX data (filled boxes) are taken from Ref. [31].

significant enhancement above 1 for $p_t^e = 1 \sim 3$ GeV,

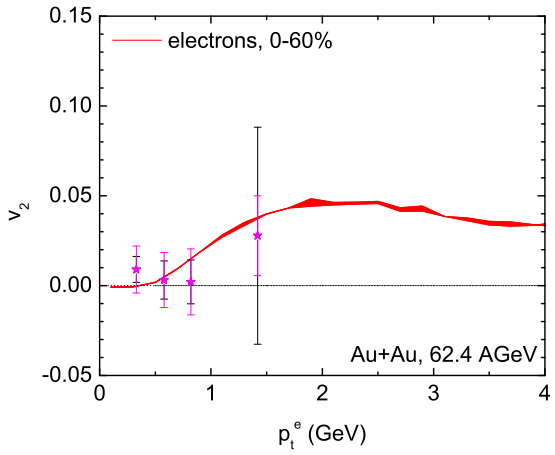

FIG. 9: (Color online) Total HF electron v_2 in 0-60% central Au+Au($\sqrt{s_{\rm NN}}$=62.4 GeV), calculated from a $N_{\rm coll}$-weighted average of v_2's of the 0-20%, 20-40% and 40-60% bins. STAR data (filled stars) are taken from Ref. [58].

as a genuine signature of the stronger flow bump in the $R_{\rm AA}$ for central relative to peripheral collisions. At the same time, and as a necessary consequence, the stronger suppression in more central collisions still manifests itself at higher p_t^e>5 GeV, although the quenching is somewhat counteracted by the Cronin effect. The current PHENIX data for $R_{\rm CP}$ support this trend, albeit again with large uncertainties.

Finally we compare our calculated HF electron v_2 with PHENIX data for 3 centralities (0-20%, 20-40% and 40-60%) in Fig. 8, and with STAR data for 0-60% centrality in Fig. 9. The latter is calculated from a $N_{\rm coll}$-weighted average of v_2's of the former 3 centrality bins. Here, no discrepancy with the data can be made out, albeit within rather large experimental uncertainties at this point. It would be illuminating to scrutinize the agreement with higher precision data. As emphasized in our previous works [16, 59], the maximum interaction strength around $T_{\rm pc}$ in our microscopic T-matrix model for HF diffusion, together with a build-up time of the bulk-v_2 of a few fm/c, implies the HF v_2 to be more sensitive to the pseudo-critical region than the $R_{\rm AA}$. We expect this sensitivity to be enhanced at lower collision energies (but the latter should still be high enough for the medium evolution to comfortably encompass the transition region).

IV. SUMMARY

We have conducted a study of open HF probes in Au+Au collisions at $\sqrt{s_{\rm NN}}$=62.4 GeV using a nonperturbative transport model in a hydrodynamically expanding medium. Heavy-flavor diffusion is realized within the same transport approach through QGP, hadronization and hadronic matter as applied in our previous calcu-

lations at top RHIC and LHC energies [23, 30]. To the extent that the initial HQ distributions and hydrodynamic medium evolution can be controlled, our results carry predictive power. For the medium evolution, our earlier ideal-hydro tune at full RHIC energy (utilizing an initial flow and compact entropy density profile) was adapted to reproduce measured pion and proton spectra and v_2 at 62.4 GeV, with acceptable precision for our HF estimates. For the initial-state Cronin effect, we took guidance from theoretical expectations with numerical values motivated by experiments at full RHIC energy. The suppression and flow pattern of the HF decay electrons at 62.4 GeV emerges from an interplay of the Cronin enhancement and the partial thermalization of heavy flavor in the hot medium starting from a softer *pp* baseline than at 200 GeV. In particular, the role of resonance recombination, characterizing the strong HF-medium coupling around the pseudo-critical region, has been identified as the main source for developing a rather pronounced "flow bump" in the electron $R_{\rm AA}$. Within the currently rather large experimental uncertainties, our predictions are roughly compatible with the PHENIX data, with a tendency to underestimate the yields at high p_t^e in central collisions and overestimate them at low p_t^e in peripheral ones. Whether these discrepancies are due to the transport treatment or initial-state effects remains an open question. On the other hand, our results for the $R_{\rm CP}$, which is less sensitive to uncertainties in the initial spectra from *pp*, agree with the data reasonably well, and still exhibit a transition from a flow bump at low p_t^e to a net suppression at high p_t^e. No discrepancies were found with the v_2 data, where our calculations yield values comparable to full RHIC energy. Our analysis is not incompatible with the formation of a QCD medium in Au+Au collisions at 62.4 GeV, whose strong coupling around the pseudo-critical region imparts substantial collectivity on HF particles through their nonperturbative interactions. However, more precise data would allow for much more sensitive tests of the pertinent structures emerging from our calculations.

Acknowledgments

We are indebted to F. Riek and K. Huggins for providing the results for the HQ transport coefficients, to W. Xie and M. Mustafa for providing the STAR data, and to J. M. Durham and A. Lebedev for providing the PHENIX data. This work was supported by the U.S. National Science Foundation (NSF) through CAREER grant PHY-0847538 and grant PHY-1306359, by the A.-v.-Humboldt Foundation, by the JET Collaboration and DOE grant DE-FG02-10ER41682, and by NSFC grant 11305089.

[1] N. Armesto, A. Dainese, C. A. Salgado and U. A. Wiedemann, Phys. Rev. D **71**, 054027 (2005) [hep-ph/0501225].
[2] Y. L. Dokshitzer and D. E. Kharzeev, Phys. Lett. B **519**, 199 (2001).
[3] R. Rapp and H. van Hees, in *Quark-Gluon Plasma 4* (R. Hwa and X.N. Wang, eds.), World Scientific (Singapore, 2010) 111 [arXiv:0903.1096 [hep-ph]].
[4] B.I. Abelev *et al.* [STAR Collaboration], Phys. Rev. Lett. **98** 1,92301 (2007); [Erratum-ibid. **106**, 159902 (2011)].
[5] A. Adare *et al.* [PHENIX Collaboration], Phys. Rev. Lett. **98**, 172301 (2007).
[6] A. Adare *et al.* [PHENIX Collaboration], Phys. Rev. C **84**, 044905 (2011).
[7] B. Abelev *et al.* [ALICE Collaboration], JHEP **1209**, 112 (2012).
[8] B. Abelev *et al.* [ALICE Collaboration], Phys. Rev. Lett. **111**, 102301 (2013).
[9] S. Sakai *et al.* [ALICE Collaboration], Nucl. Phys. A **904-905**, 661c (2013).
[10] B. B. Abelev *et al.* [ALICE Collaboration], arXiv:1405.2001 [nucl-ex].
[11] S. Chatrchyan *et al.* [CMS Collaboration], JHEP **1205**, 063 (2012).
[12] CMS Collaboration, CMS-PAS-HIN-12-014.
[13] H. van Hees, V. Greco and R. Rapp, Phys. Rev. C **73**, 034913 (2006).
[14] G.D. Moore and D. Teaney, Phys. Rev. C **71**, 064904 (2005).
[15] B. Zhang, L.-W. Chen and C. -M. Ko, Phys. Rev. C **72**, 024906 (2005).
[16] H. van Hees, M. Mannarelli, V. Greco and R. Rapp, Phys. Rev. Lett. **100**, 192301 (2008).
[17] P.B. Gossiaux, R. Bierkandt and J. Aichelin, Phys. Rev. C **79**, 044906 (2009).
[18] Y. Akamatsu, T. Hatsuda and T. Hirano, Phys. Rev. C **79**, 054907 (2009).
[19] S. Mazumder, T. Bhattacharyya, J.-e Alam and S.K. Das, Phys. Rev. C **84**, 044901 (2011) .
[20] J. Uphoff, O. Fochler, Z. Xu and C. Greiner, Phys. Rev. C **84**, 024908 (2011).
[21] W.M. Alberico, A. Beraudo, A. De Pace, A. Molinari, M. Monteno, M. Nardi and F. Prino, Eur. Phys. J. C **71**, 1666 (2011).
[22] M. He, R.J. Fries and R. Rapp, Phys. Rev. C **86**, 014903 (2012).
[23] M. He, R.J. Fries and R. Rapp, Phys. Rev. Lett. **110**, 112301 (2013).
[24] J. Aichelin, P.B. Gossiaux and T. Gousset, Acta Phys. Polon. B **43**, 655 (2012).
[25] J. Uphoff, O. Fochler, Z. Xu and C. Greiner, Phys. Lett. B **717**, 430 (2012).
[26] M. He, R.J. Fries and R. Rapp, Nucl. Phys. A **910**, 409 (2013).
[27] T. Lang, H. van Hees, J. Steinheimer and M. Bleicher, arXiv:1211.6912 [hep-ph].
[28] W.M. Alberico, A. Beraudo, A. De Pace, A. Molinari, M. Monteno, M. Nardi, F. Prino and M. Sitta, Eur. Phys. J. C **73**, 2481 (2013).

[29] S. Cao, G.-Y. Qin and S.A. Bass, Phys. Rev. C **88**, 044907 (2013).
[30] M. He, R. J. Fries and R. Rapp, Phys. Lett. B **735**, 445 (2014).
[31] A. Adare *et al.* [PHENIX Collaboration], arXiv:1405.3301 [nucl-ex].
[32] M. Mustafa *et al.* [STAR Collaboration], Nucl. Phys. A **904-905**, 665c (2013), and M. Mustafa, private communication (2014).
[33] A. Adare *et al.* [PHENIX Collaboration], Phys. Rev. Lett. **109**, 152301 (2012).
[34] A. Adare *et al.* [PHENIX Collaboration], Phys. Rev. Lett. **109**, 242301 (2012).
[35] F. Riek and R. Rapp, Phys. Rev. C **82**, 035201 (2010).
[36] M. He, R. J. Fries and R. Rapp, Phys. Lett. B **701**, 445 (2011).
[37] K. Huggins and R. Rapp, Nucl. Phys. A **896**, 24 (2012).
[38] F. Riek and R. Rapp, New J. Phys. **13**, 045007 (2011).
[39] L. Ravagli and R. Rapp, Phys. Lett. B **655**, 126 (2007).
[40] E. Braaten, K.-m. Cheung, S. Fleming and T.C. Yuan, Phys. Rev. D **51**, (1995) 4819.
[41] V.G. Kartvelishvili, A.K. Likhoded and V.A. Petrov, Phys. Lett. B **78**, 615 (1978).
[42] P.F. Kolb and W. Heinz, In *Hwa, R.C. (ed.) et al.: Quark gluon plasma* 634-714, [nucl-th/0305084].
[43] H. van Hees, M. He and R. Rapp, arXiv:1404.2846 [nucl-th].
[44] M. He, R.J. Fries and R. Rapp, Phys. Rev. C **85**, 044911 (2012).
[45] B.I. Abelev *et al.* [STAR Collaboration], Phys. Lett. B **655**, 104 (2007).
[46] L. Adamczyk *et al.* [STAR Collaboration], Phys. Rev. C **88**, 014902 (2013).
[47] M. Cacciari, S. Frixione and P. Nason, JHEP **0103**, 006 (2001).
[48] I. Vitev, J. T. Goldman, M. B. Johnson and J. W. Qiu, Phys. Rev. D **74**, 054010 (2006).
[49] Hard Probe Collaboration (R. Vogt *et al.*),, Int. J. Mod. Phys. E **12**, 211 (2003).
[50] J. Hufner and P. f. Zhuang, Phys. Lett. B **515**, 115 (2001)
[51] N. S. Topilskaya *et al.* [NA50 Collaboration], Nucl. Phys. A **715**, 675 (2003).
[52] A. Adare *et al.* [PHENIX Collaboration], Phys. Rev. C **77**, 024912 (2008).
[53] X. Zhao and R. Rapp, Phys. Rev. C **82**, 064905 (2010)
[54] X. N. Wang, Phys. Rev. Lett. **81**, 2655 (1998).
[55] R. C. Hwa and C. B. Yang, Phys. Rev. Lett. **93**, 082302 (2004).
[56] P. M. Chesler, M. Lekaveckas and K. Rajagopal, JHEP **1310**, 013 (2013).
[57] L. Adamczyk *et al.* [STAR Collaboration], arXiv:1404.6185 [nucl-ex].
[58] L. Adamczyk *et al.* [STAR Collaboration], arXiv:1405.6348 [hep-ex].
[59] R. Rapp, J. Phys. G **36**, 064014 (2009).